Fabrication of birefringent nanocylinders for single-molecule force and torque measurement

2014 Nanotechnology 25 235304

(http://iopscience.iop.org/0957-4484/25/23/235304)

IOP Publishing Nanotechnology
Nanotechnology **25** (2014) 235304 (8pp) doi:10.1088/0957-4484/25/23/235304

Fabrication of birefringent nanocylinders for single-molecule force and torque measurement

Ping-Chun Li[1,3], Jen-Chien Chang[2,3], Arthur La Porta[2] and Edward T Yu[1]

[1] Microelectronics Research Center, 10100 Burnet Road, Austin, TX 78758, USA
[2] Department of Physics, Institute for Physical Science and Technology, University of Maryland, College Park, MD 20742, USA

E-mail: ety@ece.utexas.edu

Received 9 January 2014, revised 20 March 2014
Accepted for publication 7 April 2014
Published 21 May 2014

Abstract

Optically anisotropic subwavelength scale dielectric particles have been shown to enable studies of the mechanical properties of bio-molecules via optical trapping and manipulation. However, techniques emphasized to date for fabrication of such particles generally suffer from limited uniformity and control over particle dimensions, or low throughput and high cost. Here, an approach for rapid, low-cost, fabrication of large quantities of birefringent quartz nanocylinders with dimensions optimized for optical torque wrench experiments is described. For a typical process, 10^8 or more quartz cylinders with diameters of 500 nm and heights of 800 nm, with uniformity of ±5% in each dimension, can be fabricated over ~10 cm^2 areas, for binding to a single bio-molecule, and harvested for use in optical trapping experiments. Use of these structures to measure extensional and torsional dynamics of single DNA molecules is demonstrated with measured forces and torques shown to be in very good agreement with previously reported results.

S Online supplementary data available from stacks.iop.org/NANO/25/235304/mmedia

Keywords: optical tweezer, nanosphere lithography, subwavelength optics

(Some figures may appear in colour only in the online journal)

1. Introduction

Techniques such as optical tweezers [1–3], magnetic tweezers [4], atomic force microscopy [5], and fluorescence microscopy [6] have been developed to manipulate and observe single bio-molecules, enabling rare and transient events to be observed by avoiding averaging that occurs in traditional ensemble measurements. Among these, optical tweezers have been used to characterize various bio-molecules and biological processes in measurements of force and displacement in piconewton and sub-nanometer regime. Examples include measuring mechanical properties of biopolymers, reconstructing energy landscapes for folding or unfolding secondary structure of nucleic acids, and directly following dynamics of motor proteins translocating on their tracks [7–11]. While most experiments characterize force and displacement, torque and angular motion play significant roles in biological phenomena such as DNA replication and transcription [12], ATP synthesis [13] or bacteria propulsion [14, 15]. However, there have been relatively few reports on torque and angular measurements of bio-molecules due to limited availability of methods to directly manipulate and detect such quantities. Here, we present a method to fabricate large quantities of birefringent cylinders rapidly and at low cost using nanosphere lithography (NSL), [16–18] and demonstrate their use for single-molecule experiments using an optical torque wrench (OTW) measurement. Key design considerations are described and compared with other methods, with nanocylinders of diameter ~500 nm and height ~800 nm shown to provide stable angular trapping in OTW.

[3] These authors contributed equally to this work.

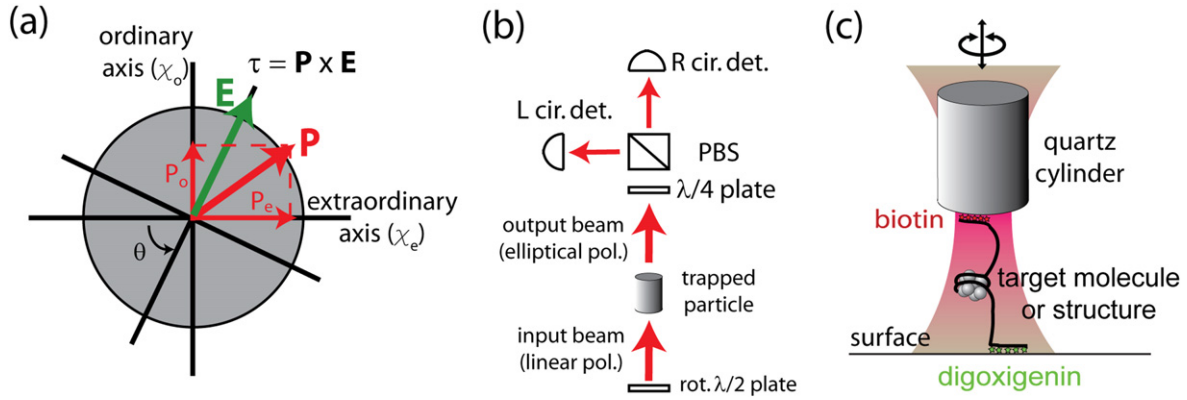

Figure 1. (a) Schematic diagram of a birefringent particle whose extraordinary axis is misaligned with the external electric field (E). Torque is generated when the induced polarization (P) is not aligned with the electric field (E). The angle between electric field and extraordinary axis (χ_e) is denoted as θ. (b) Schematic diagram of the torque detection in OTW. The torque signal is measured by detecting the imbalance of left- and right-circular polarized components of the scattered beam. PBS: polarizing beam splitter. (c) Schematic of OTW setup using fabricated quartz cylinders for single molecule experiments. The force and torque exerted on the bio-molecule are controlled by adjusting the polarization state of laser and the surface position.

Finally, force and torque generated using the cylinders are calibrated, and linear and angular manipulations of twist–stretched DNA are demonstrated and discussed. We anticipate that the fabrication approach described here, which enables rapid, flexible, low-cost production of dielectric nanostructures with dimensions of <100 nm to ~1000 nm [17] will help facilitate broad access to optical tweezers, OTW, and related measurements in single-molecule biophysics.

The OTW [19] has been developed for angular manipulation and precise detection of torque via an optically anisotropic particle trapped in a laser beam. Figure 1(a) shows a birefringent particle whose ordinary axis (χ_o) and extraordinary axis (χ_e) are misaligned to an external electric field. As a consequence, a restoring torque (τ) from the cross product of induced polarization (P) and external electric field (E) tends to align the extraordinary axis with the external electric field. The resulting torque can be expressed as

$$\tau = \left|\vec{P} \times \vec{E}\right| = \frac{1}{2}(\chi_0 - \chi_e)\mathrm{E}\ \sin 2\theta = \tau_0\ \sin 2\theta, \qquad (1)$$

where θ is the angle between electric field and extraordinary axis, and τ_0 is the maximum magnitude of torque which can be exerted on the particle. The torque signal can be determined by measuring the spin angular momentum transfer of the photon, i.e. imbalance of left- and right-circular components of the transmitted beam as shown in figure 1(b). Figure 1(c) shows a typical OTW setup for single-molecule experiments. The target bio-molecule is attached with one end to the glass slide and the other end to a birefringent particle trapped by a tightly focused Gaussian beam. Controlling the position of the surface and the state of the input laser beam allows us to simultaneously stretch and rotate the molecule. The multiple attachments make the torsion added to the molecule possible. Force and torque response is detected by monitoring the position and polarization state of the transmitted trap beam.

A number of studies have been reported on design and fabrication of optimal particles in OTW [20–25]. The requirement of optical anisotropy can be obtained from shape or material. In the case of form birefringence, the difference in dimensions and resulting anisotropy of polarizability make angular trapping possible, as reported for oblate particles [23]. However, it is difficult to obtain the uniformity of size and shape which is necessary for precise calibration in single-molecule experiments. In an alternate approach, birefringent quartz cylinders have been designed and fabricated for use in OTW, and offer several advantages. First, the fabrication processes makes them easy to produce in large quantity and with high uniformity. Second, the elongated shape allows the symmetric axis of the cylinder to align with the propagation direction of the incident light, leaving the only rotational degree of freedom to be controlled by the external field. Finally, for use in single-molecule experiments, the cylinder can be selectively functionalized only on the top surface, increasing the efficiency in achieving the appropriate geometry for measurement. In previous reports, fabrication of such cylinders was achieved by optical [20, 21] or electron beam lithography [22]. However, these fabrication methods are either restricted in minimum feature size due to diffraction limit or are extremely time-consuming, and generally very expensive. Here, we implement a fabrication process for quartz cylinders suitable for OTW experiments using NSL. NSL has been previously developed and applied in anti-reflection coatings, sensing, and solar energy harvesting [26–30]. We adapt the NSL technique and fabricate quartz nanocylinders with tunable sizes.

2. Experiments

The size of nanocylinders typically must be optimized according to the specific application. For example, larger nanocylinders can provide larger torque under same laser intensity and are suitable for experiments such as bacterial flagellar motor which is capable of generating torque up to 4000 pN nm [31]. On the other hand, smaller nanocylinders

offer faster response time and can be applied to molecular motors that do not generate large torque such as ATPase or RNA polymerase [12, 13]. NSL readily provides the necessary flexibility in size of birefringent nanocylinders, enabling more possibilities to be explored rapidly and easily in single-molecule experiments by OTW. Figure 2 shows the key steps in the fabrication process for the birefringent nanocylinders. Starting from a 4″ single crystal quartz (X-cut) substrate, 90 nm Cr/10 nm SiO_2 are deposited by e-beam evaporation. A self-assembled monolayer of 2 μm diameter polystyrene (PS) nanospheres (with standard deviation of 27 nm as determined from analysis of scanning electron micrograph) is then deposited on the SiO_2 surface using the Langmuir–Blodgett method [16, 17] as shown in figure 2(a). Reactive ion etching (RIE) is used to etch the PS spheres to reduce the diameter to 1–1.5 μm. These nanospheres then serve as an etch mask to transfer the hexagonal pattern to the underlying Cr, which acts as a hard mask containing Cr discs with diameter 510 nm (with standard deviation of 20 nm) as shown in figure 2(b). The quartz substrate with Cr hard mask on top then underwent RIE to yield quartz pillars 800 nm (with standard deviation of 22 nm) in height as shown in figure 2(c). The Cr mask and residual polymer resulting from the dry etch are removed by a standard wet etch process. NSL enables fabrication of dielectric nanostructures over a broad range of sizes, and specific dimensions can be readily achieved by changing the initial nanosphere diameter in details of the etching process employed. The diameter of the nanocylinders can range from 50 nm to 1 μm depending on the size of the spheres and total etching time, and the height of the nanocylinders ranges from 500 nm to 2 μm, depending on the thickness of Cr mask. We note that the torque in OTW experiment is proportional to the volume of the nanocylinder since the signal strength depends on the total angular momentum transfer of the nanocylinder. The aspect ratio of the nanocylinder should be also large enough to enable the alignment of the long axis of the nanocylinder with the laser beam. With these considerations, birefringent quartz nanocylinders with diameter 500 nm and height 800 nm have been found to be suitable for single-molecule experiment in OTW, and this size range was targeted for our experiment [20].

As shown in figure 2(d), the patterned substrate is then spin coated with PMMA, and the excess PMMA etched away so that only the top surfaces of the nanocylinders are exposed. For application in single-molecule experiments, we selectively functionalize only the top surface of the nanocylinder with amino group which is necessary for further avidin coating. Next, the wafer is incubated in 1% Vectabond reagent (Vector Laboratories) for 5 min and then transferred to acetone for 30 min to remove the PMMA. The wafer is air-dried and cylinders are collected using a microtome blade (C. L. Sturkey) as shown in figures 2(e)–(g). Finally, Avidin (Vector Laboratories) molecules are coupled to the amino-functionalized cylinders using a Glutaraldehyde kit (Polysciences). For the experiment measuring twist–stretched DNA, the rotationally-constrained DNA is ligated from three pieces made separately by polymerase chain reaction. The central piece is 1351 bp. Two short pieces incorporate multiple digoxigenin (322 bp) and biotin (336 bp) labelled nucleotides, which allows for torsionally constrained binding to the sample chamber surface and cylinder respectively. The detailed protocol for sample chamber creation and DNA binding to the surface and cylinder is similar to previous methods with PS sphere [32, 33]. Briefly, the cover slip surface is coated with anti-digoxigenin, followed by blotting buffer to prevent non-specific sticking of DNA and cylinder. DNA and nanocylinder are then incubated, respectively. Finally, the sample are flowed and left with experimental buffer solution (50 mM sodium phosphate buffer pH 7.0, 50 mM NaCl, 10 mM EDTA, 0.02% Tween 20, and oxygen scavenger solution). We note that controlling the distance between each nanocylinder and the aspect ratio is crucial to avoid incomplete removal of the nanocylinders and undesired quartz residues. Using this process, a 4″ quartz wafer provides ~10^8 nanocylinders, which is sufficient for calibration and measurement in a typical single-molecule experiment. Compared with conventional lithographies, the approach described here provides a rapid, low-cost, large-area nanoscale patterning technique covering a wide range of sizes.

Figure 3(a) shows the distribution of nanocylinder diameter collected from different radial positions away from the 4″ wafer center. The overall distributions for different positions are uniform and consistent with a normal distribution except for a few outliers due to imperfect distribution of the PS nanospheres. Figure 3(c) shows the overall distribution of nanocylinder diameter. The averaged diameter is 510 nm with standard deviation of 20 nm. We observe the diameters of the nanocylinders at the center of the wafer are smaller than other places due to lateral etching from variations of local plasma density during RIE process. Figure 3(b) shows the distribution of nanocylinder height collected from different position from the 4″ wafer center. The heights of the nanocylinders are overall uniform. Figure 3(d) shows the overall distribution of nanocylinder height. The averaged height is 800 nm with standard deviation of 22 nm. These results confirm that, NSL can provide large numbers of birefringent nanocylinders with excellent uniformity.

3. Results and discussion

Accurate calibration of force and torque is required to perform precise quantitative measurements for a trapped nanocylinder in OTW. For cylinders of the size discussed here, the calibration of force and position follows the standard protocol for PS particles of similar dimensions in optical tweezers experiments [3]. Analogous to force, the calibration of torque and rotation can be achieved by measuring the power spectrum of the torque signal (intensity difference in two detectors) for a trapped nanocylinder [19, 20, 34]. The power spectrum can be fitted by a Lorentzian line shape due to Brownian fluctuations in rotational motion [35]. This Lorentzian characteristic is modelled as $P(f) = A^2/(f^2 + f_0^2)$ with corner frequency $f_0 = \alpha/2\pi\xi$, and amplitude $A^2 = kT/\pi^2\alpha$, where α is the stiffness of the angular trap, ξ is rotational drag coefficient, k is

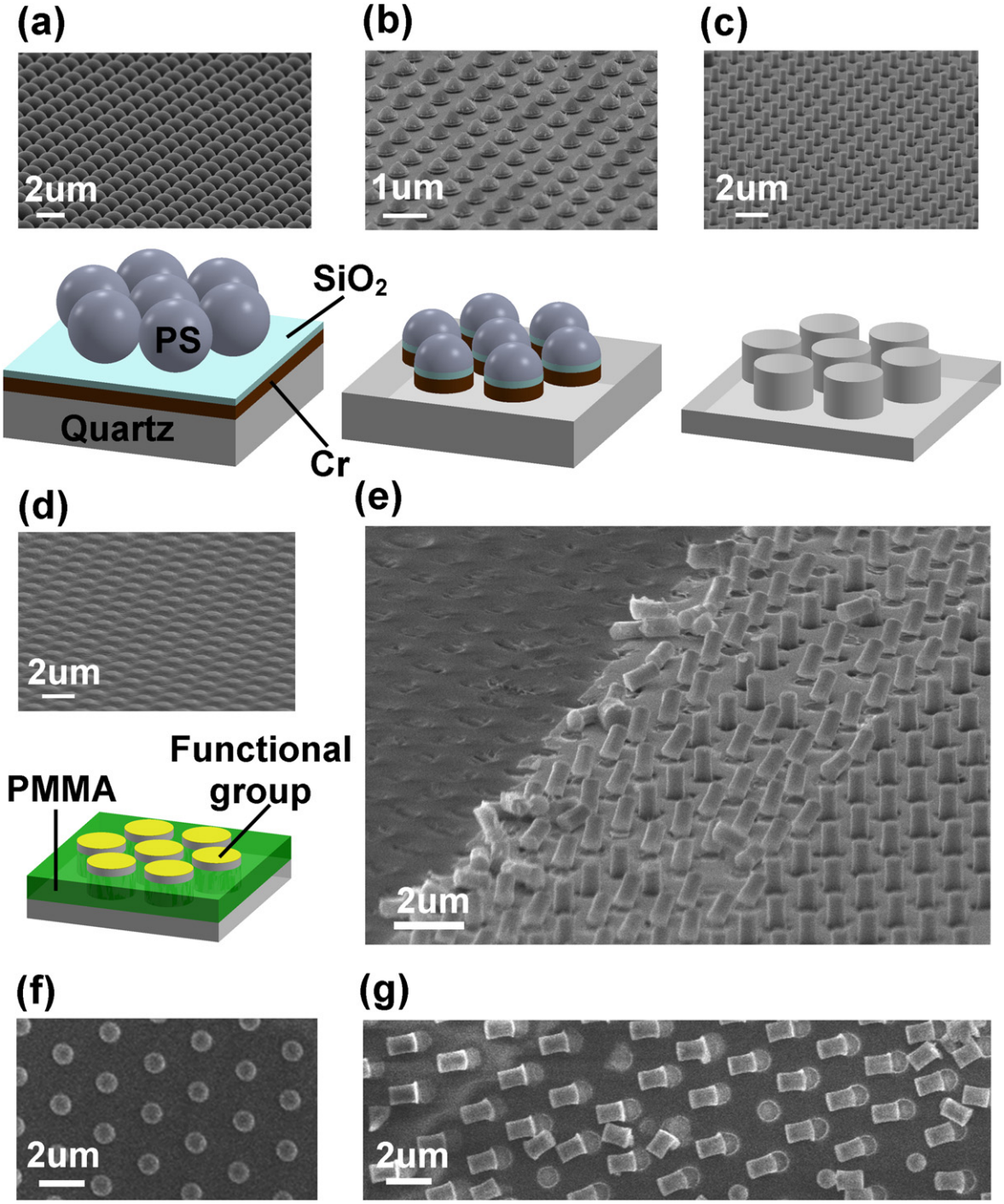

Figure 2. Schematic diagram of the fabrication process flow and scanning electron micrograph at each step. (a) A single crystal quartz substrate is covered with 10 nm Cr/100 nm SiO_2, followed by NSL using 2 μm diameter PS nanospheres. (b) A series of dry etching processes is used to reduce the sphere size and transfer the hexagonal lattice pattern to the underlying Cr layer. (c) Nanocylinders formed from single crystal quartz by dry etching using Cr mask, which is later removed by wet etch process. (d) Nanocylinder buried in PMMA with only the top surface exposed for amino-group functionalization. (e) Tilted view of single quartz nanocylinders after mechanical removal. (f)–(g) Top-down views of single crystal quartz nanocylinders before and after mechanical removal.

the Boltzmann constant, and T is temperature in Kelvin. In figure 4(a) we observe that the measured power spectrum for a birefringent nanocylinder (solid squares) is in good agreement with the fitted Lorentzian line (solid line), showing the birefringent nanocylinder is angularly trapped; whereas a 820 nm diameter PS nanosphere (solid circles) is not trapped due to the lack of birefringence. The angular sensitivity is measured by rotating polarization on a cylinder fixed to the surface. Figure 4(b) shows that the torque signal modulates sinusoidally, where θ rotating at 1.8 rad s^{-1} is the angle between the direction of electric field and the extraordinary axis of the nanocylinder as shown in figure 1(a), and V_0 is the maximum

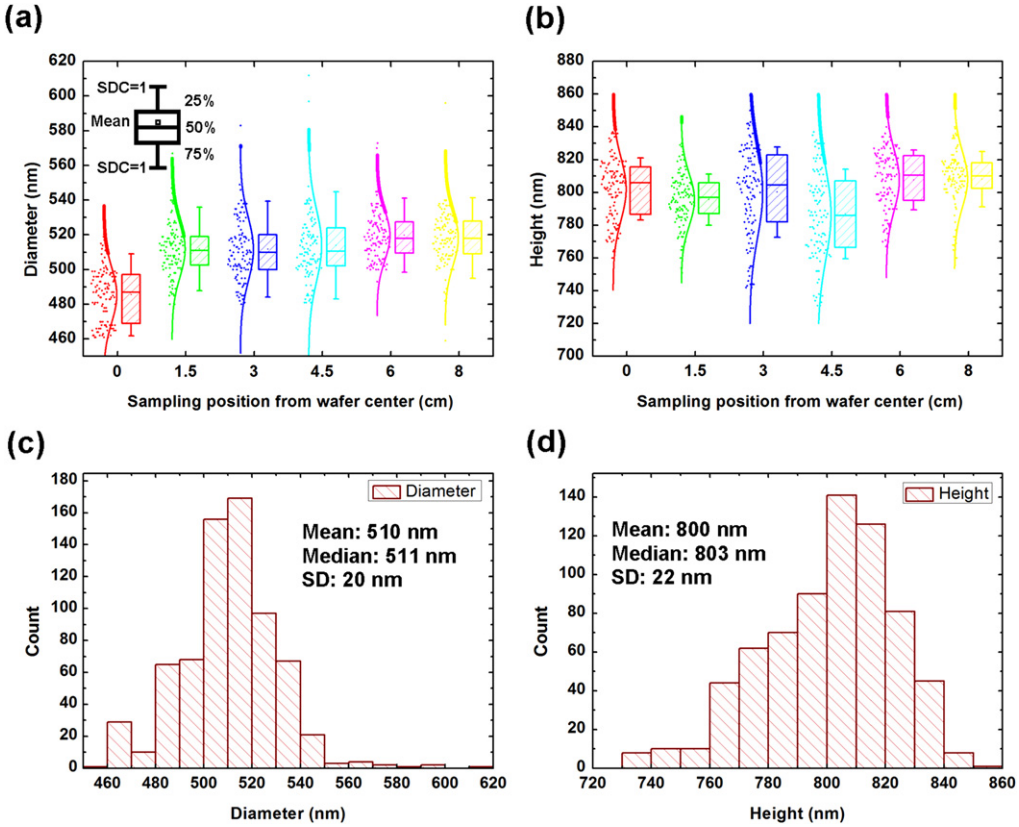

Figure 3. (a)–(b) Distribution and box chart of nanocylinder diameter and height as a function of position from wafer center. The top and bottom of the box are the first and third quartiles. The median and mean are shown as the band and square symbol inside the box. The top and bottom whiskers stand for the standard deviation coefficient (SDC) equal to 1. (c)–(d) Overall distributions of nanocylinder diameter and height with values for mean, median, and standard deviation for each.

torque signal voltage obtained at $\theta = 45°$. Using the fitted parameters $f_0 = 204$ Hz and $A^2 = 9.8 \times 10^{-5}$ V^2 Hz from data shown in figure 4(a) as well as $V_0 = 0.11$ V in figure 4(b), we obtain $\xi = 2.1$ pN nm s, $\alpha = 2.6 \times 10^3$ pN nm rad^{-1}, and torque signal sensitivity 1.2×10^5 pN nm V^{-1}. The measured torque signal can therefore be obtained by

$$\tau = \alpha\theta = \alpha\left(V_\tau / 2V_0\right). \tag{2}$$

The maximum torque which can be generated here is ~1300 pN nm, given the nominal laser power ~300 mW Teasured before rotational half-wave plate. We note the experimentally determined rotational drag coefficient here is consistent with other experimental [32] and theoretical works [36] for nanocylinders with similar dimensions.

We further demonstrate the application of the birefringent nanocylinder in single-molecule experiments by measuring a twisted and stretched DNA undergoing structural transition. The twisted state of DNA is regulated *in vivo* by topoisomerases and influences the accessibility of DNA to many motor proteins. Therefore the mechanical properties of DNA under tension and torsion have profound implications in many biological contexts. Figure 4(c) shows the measured and theoretically modeled extension of dsDNA recorded as a function of numbers of rotations under different stretching forces. Positive rotation is defined as the direction to overwind dsDNA. With positive torsion, the extension curves remain constant at low total turns (<3) since dsDNA is only overtwisted slightly. Beyond this region, the extension of dsDNA starts to drop abruptly and monotonically as total turns are added, indicating that the dsDNA buckles to form a plectoneme. The critical number of turns for this sharp transition increases with the applied force due to the increased rigidity of dsDNA under tension. Our observations are also confirmed with the phenomenological model for dsDNA phase transition under force and torque via minimization of total free energies for combinations of different states (see supporting information for detailed descriptions and discussions, available at stacks.iop.org/NANO/25/235304/mmedia). In brief, for a pure state (i) of dsDNA, the free energy of each state can be approximated as a function of linking number density (σ) and force (f) [37, 38],

$$G_i(\sigma, f) = \varepsilon_i - g_i(f) + \frac{c_i(f)(\sigma - \sigma_{0,i})^2}{2}, \tag{3}$$

where ε_i is the energy offset, $\sigma_{0,i}$ is the relaxed linking number, $c_i(f)$ and $g_i(f)$ are the torsional coefficient and stretching energies as functions of force which can be

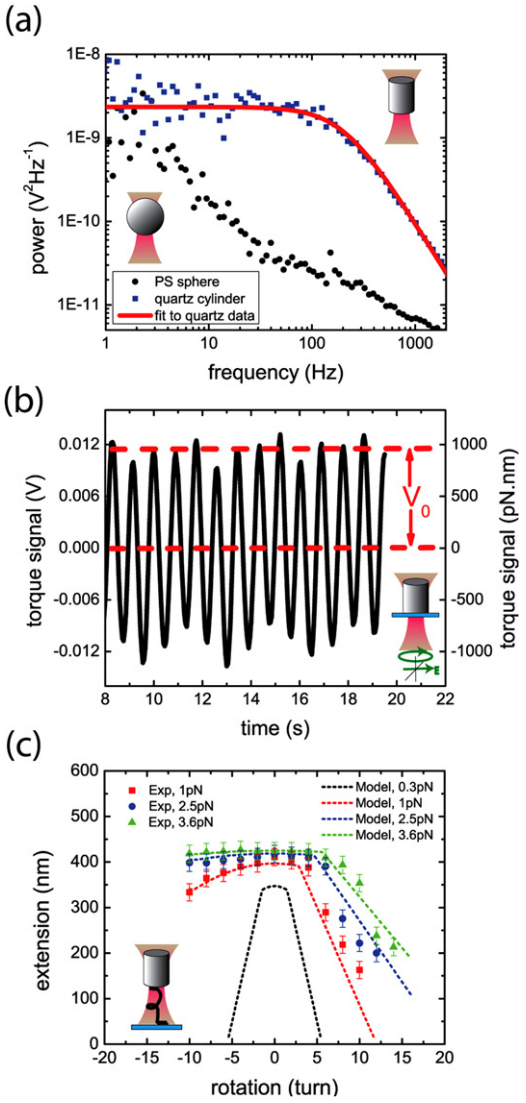

Figure 4. (a) Measured power spectra of torque signal for birefringent nanocylinders and polystyrene spheres with diameter of 820 nm. The solid line indicates the Lorentzian fit for birefringent nanocylinders. (b) Torque signal of a fixed birefringent nanocylinder scanned by a rotating polarization vector. (c) Measured rotation–extension curve for a double-stranded DNA at different fixed forces. Gray dashed line indicates model prediction for low force limit.

expressed as,

$$c_i(f) = C_i kT\omega_0^2\left(1 - \frac{C_i}{4A_i}\sqrt{\frac{kT}{A_i f}}\right), \tag{4}$$

and

$$g_i(f) = \lambda_i\left(f - \sqrt{\frac{kTf}{A_i}}\right), \tag{5}$$

respectively, where k is the Boltzmann constant, T is the temperature (which we assume it is under room temperature, 300 K), $\omega_0 = 2\pi/3.6\,\text{nm} = 1.85\,\text{nm}^{-1}$ is the contour-length rate of rotation of the relaxed double helix, and A_i and C_i are the stretched and twist persistence length, respectively. Between the phase transition from one state to the other, the dsDNA can also form into coexisting states between two pure states if the free energy of the mixed state is lower than the other pure states. The free energy for a coexisting state between i and j state can be expressed as [37],

$$G_{i-j} = x_i G_i(\sigma_i) + x_j G_j(\sigma_j), \tag{6}$$

where x_i and, x_j are the fraction of i and j state, respectively under the constraint, $x_i + x_j = 1$. These quantities can be expressed as,

$$x_i = \frac{\sigma_j - \sigma}{\sigma_j - \sigma_i} \quad \text{and} \quad x_j = \frac{\sigma - \sigma_i}{\sigma_j - \sigma_i}. \tag{7}$$

The onset and end linking number densities, σ_i, and σ_j, can be calculated by minimization of coexistence free energy $\left(\frac{\partial G_{i-j}}{\partial \sigma_i} = 0\right)$ with the constraint $\sigma = x_i\sigma_i + x_j\sigma_j$. Finally the modeled free energy (G_i) and linking number density (σ) can be converted into experimentally measured quantity as extension (z) and rotation turn as shown in figure 3(c), respectively, by [37]

$$\frac{z}{L} = -\frac{\partial G_i}{\partial f}, \tag{8}$$

and

$$\sigma = \frac{\Delta Lk}{Lk_0} = \frac{n}{L/h}, \tag{9}$$

where Lk_0 is the normalized linking number of the relaxed dsDNA, $L = 1351$ bp is the total length of DNA studied here, $h = 10.5$ bp is the contour length of a single helix, and n is the number of rotation turns. Figure 4(c) shows that for low positive rotation turns ($n < 3$), the parabolic trend from equation (3) can be observed from both modeled and measured results, and is followed by the onset of the coexistence of stretched and plectonemic states. The modeled extension of dsDNA decreases linearly to zero where it reaches the full plectonemic state, and this trend is consistent with our measured results for all applied forces, except for dsDNA still have physical length due to imperfect supercoiling in realistic situation. Upon negative rotation, the extension responses with higher force (2.5 and 3.6 pN) remain almost constant because dsDNA prefers to unwind rather than buckle, therefore no plectoneme is formed. For lower force (1 pN), the dsDNA unwinds and buckles simultaneously when the total applied turn increases so that the extension curve drops without a sharp transition. These characteristics can be understood by the coexistence of stretched and denatured states by following the similar derivation based on equation (3) (see supporting information for more details). For even lower force (0.3 pN), a symmetric extension response is expected based on the phase transition model [37]. The force is small enough that unwinding of helix structure is unfavorable and only the stretched and plectonemic states are allowed. The characteristics we observe in these measurements are

consistent with other measurements performed using magnetic tweezers [39, 40] and OTW [41, 42].

In conclusion, a method for fabricating large quantities of birefringent nanocylinders using low-cost, rapid-patterning NSL, and their use in single-molecule manipulation of dsDNA with OTW, are demonstrated. Patterning of the cylinder structures using NSL offers a number of advantages over conventional lithographies employed in previous approaches, most notably in enabling rapid low cost fabrication of very large numbers of dielectric nanocylinders as required in OTW experiments. The calibration of force and torque in OTW measurements using dielectric nanocylinders fabricated in this way, together with the measured and modelled extension curve of double-stranded DNA under positive and negative rotation confirm the applicability of these birefringent nanocylinders in OTW measurements.

Acknowledgements

This work has been partially supported by the National Science Foundation (ECCS-1120823) and the Judson S Swearingen Regents Chair in Engineering at the University of Texas at Austin (to ETY), and by Maryland Technology Development Corporation (to ALP). P-C Li would like to thank H-H Kung (Rutgers University) and E-S Liu (UT-Austin) for detailed discussions on NSL and fabrication process.

References

[1] Ashkin A 1970 Acceleration and trapping of particles by radiation pressure *Phys. Rev. Lett.* **24** 156–9
[2] Ashkin A, Dziedzic J M, Bjorkholm J E and Chu S 1986 Observation of a single-beam gradient force optical trap for dielectric particles *Opt. Lett.* **11** 288–90
[3] Neuman K C and Block S M 2004 Optical trapping *Rev. Sci. Instrum.* **75** 2787–809
[4] Tanase M, Biais N, Sheetz M, Yu L W and Dennis E D 2007 *Methods in Cell Biology* (New York: Academic) pp 473–93
[5] Lee C-K, Wang Y-M, Huang L-S and Lin S 2007 Atomic force microscopy: determination of unbinding force, off rate and energy barrier for protein–ligand interaction *Micron* **38** 446–61
[6] Moerner W E and Fromm D P 2003 Methods of single-molecule fluorescence spectroscopy and microscopy *Rev. Sci. Instrum.* **74** 3597–619
[7] Ashkin A and Dziedzic J 1987 Optical trapping and manipulation of viruses and bacteria *Science* **235** 1517–20
[8] Bustamante C, Cheng W and Mejia Y X 2011 Revisiting the central dogma one molecule at a time *Cell* **144** 480–97
[9] Larson M H, Landick R and Block S M 2011 Single-molecule studies of RNA polymerase: one singular sensation, every little step it takes *Mol. Cell* **41** 249–62
[10] Neuman K C and Nagy A 2008 Single-molecule force spectroscopy: optical tweezers, magnetic tweezers and atomic force microscopy *Nat. Meth.* **5** 491–505
[11] Perkins T T 2009 Optical traps for single molecule biophysics: a primer *Laser Photonics Rev.* **3** 203–20
[12] Ma J, Bai L and Wang M D 2013 Transcription under torsion *Science* **340** 1580–3
[13] Toyabe S, Watanabe-Nakayama T, Okamoto T, Kudo S and Muneyuki E 2011 Thermodynamic efficiency and mechanochemical coupling of F1-ATPase *Proc. Natl Acad. Sci.* **108** 17951–6
[14] Chen X and Berg H C 2000 Torque-speed relationship of the flagellar rotary motor of *Escherichia coli Biophys. J.* **78** 1036–41
[15] Xing J, Bai F, Berry R and Oster G 2006 Torque-speed relationship of the bacterial flagellar motor *Proc. Natl Acad. Sci. USA* **103** 1260–5
[16] Ho C-C, Chen P-Y, Lin K-H, Juan W-T and Lee W-L 2011 Fabrication of monolayer of polymer/nanospheres hybrid at a water–air interface *ACS Appl. Mater. Interfaces* **3** 204–8
[17] Kosiorek A, Kandulski W, Glaczynska H and Giersig M 2005 Fabrication of nanoscale rings, dots, and rods by combining shadow nanosphere lithography and annealed polystyrene nanosphere masks *Small* **1** 439–44
[18] Rybczynski J, Ebels U and Giersig M 2003 Large-scale, 2D arrays of magnetic nanoparticles *Colloids Surf.* A **219** 1–6
[19] La Porta A and Wang M D 2004 Optical torque wrench: angular trapping, rotation, and torque detection of quartz microparticles *Phys. Rev. Lett.* **92** 190801
[20] Deufel C, Forth S, Simmons C R, Dejgosha S and Wang M D 2007 Nanofabricated quartz cylinders for angular trapping: DNA supercoiling torque detection *Nat. Meth.* **4** 223–5
[21] Gutiérrez-Medina B, Andreasson J O L, Greenleaf W J, LaPorta A and Block S M 2010 *Methods in Enzymology* ed G W Nils (New York: Academic) pp 377–404
[22] Huang Z, Pedaci F, van Oene M, Wiggin M J and Dekker N H 2011 Electron beam fabrication of birefringent microcylinders *ACS Nano* **5** 1418–27
[23] Oroszi L, Galajda P, Kirei H, Bottka S and Ormos P 2006 Direct measurement of torque in an optical trap and its application to double-strand DNA *Phys. Rev. Lett.* **97** 058301
[24] Simpson S H and Hanna S 2007 Optical trapping of spheroidal particles in Gaussian beams *J. Opt. Soc. Am.* A **24** 430–43
[25] Simpson S H and Hanna S 2011 Optical trapping of microrods: variation with size and refractive index *J. Opt. Soc. Am.* A **28** 850–8
[26] Haynes C L and Van Duyne R P 2001 Nanosphere lithography:a versatile nanofabrication tool for studies of size-dependent nanoparticle optics *J. Phys. Chem.* B **105** 5599–611
[27] Li P-C and Yu E T 2013 Flexible, low-loss, large-area, wide-angle, wavelength-selective plasmonic multilayer metasurface *J. Appl. Phys.* **114** 133104–7
[28] Li P-C and Yu E T 2013 Large-area omnidirectional antireflection coating on low-index materials *J. Opt. Soc. Am.* B **30** 2584–8
[29] Li X H, Li P C, Hu D Z, Schaadt D M and Yu E T 2013 Light trapping in thin-film solar cells via scattering by nanostructured antireflection coatings *J. Appl. Phys.* **114** 044310–7
[30] Zhou W, Tao M, Chen L and Yang H 2007 Microstructured surface design for omnidirectional antireflection coatings on solar cells *J. Appl. Phys.* **102** 103105–9
[31] Sowa Y, Hotta H, Homma M and Ishijima A 2003 Torque–speed relationship of the Na^+-driven flagellar motor of *vibrio alginolyticus J. Mol. Biol.* **327** 1043–51
[32] de Messieres M, Brawn-Cinani B and La Porta A 2011 Measuring the folding landscape of a harmonically constrained biopolymer *Biophys. J.* **100** 2736–44
[33] Chang J C, de Messieres M and La Porta 2013 Effect of handle length and microsphere size on transition kinetics in single-molecule experiments *Phys. Rev.* E **87** 012721
[34] Pedaci F, Huang Z, van Oene M and Dekker N H 2012 Calibration of the optical torque wrench *Opt. Express* **20** 3787–802

[35] Svoboda K and Block S M 1994 Biological applications of optical forces *Annu. Rev. Biophys. Biomol. Struct.* **23** 247–85

[36] Tirado M M and de la Torre J G 1980 Rotational dynamics of rigid, symmetric top macromolecules. application to circular cylinders *J. Chem. Phys.* **73** 1986–93

[37] Marko J F 2007 Torque and dynamics of linking number relaxation in stretched supercoiled DNA *Phys. Rev.* E **76** 021926

[38] Sheinin M Y, Forth S, Marko J F and Wang M D 2011 Underwound DNA under tension: structure, elasticity, and sequence-dependent behaviors *Phys. Rev. Lett.* **107** 108102

[39] Mosconi F, Allemand J F, Bensimon D and Croquette V 2009 Measurement of the torque on a single stretched and twisted DNA using magnetic tweezers *Phys. Rev. Lett.* **102** 078301

[40] Strick T R, Allemand J-F, Bensimon D, Bensimon A and Croquette V 1996 The elasticity of a single supercoiled DNA molecule *Science* **271** 1835–7

[41] Forth S, Deufel C, Sheinin M Y, Daniels B, Sethna J P and Wang M D 2008 Abrupt buckling transition observed during the plectoneme formation of individual DNA molecules *Phys. Rev. Lett.* **100** 148301

[42] Sheinin M Y and Wang M D 2009 Twist–stretch coupling and phase transition during DNA supercoiling *Phys. Chem. Chem. Phys.* **11** 4800–3